Applied Physics Letters ARTICLE pubs.aip.org/aip/apl

Utilizing machine learning in the three-omega method to predict thermophysical properties with low variation

Cite as: Appl. Phys. Lett. **127**, 072202 (2025); doi: 10.1063/5.0274238
Submitted: 4 April 2025 · Accepted: 17 July 2025 ·
Published Online: 19 August 2025

Yasuaki Ikeda,[1] Yuki Akura,[1] Ryuto Yamasaki,[1] Yuki Matsunaga,[2] Lijun Liu,[3] Masaki Shimofuri,[1] Amit Banerjee,[1] Toshiyuki Tsuchiya,[1] and Jun Hirotani[1,a)]

AFFILIATIONS

[1]Department of Micro Engineering, Graduate School of Engineering, Kyoto University, Kyotodaigaku-katsura, Nishikyo-ku, Kyoto 615-8540, Japan
[2]Department of Chemistry, Graduate School of Science, Nagoya University, Furo-cho, Chikusa-ku, Nagoya 464-8602, Japan
[3]Department of Mechanical Engineering, Graduate School of Engineering, Osaka University, 2-1 Yamadaoka, Suita, Osaka 565-0871, Japan

[a)]**Author to whom correspondence should be addressed:** hirotani.jun.7v@kyoto-u.ac.jp

ABSTRACT

The three-omega method offers a precise and simple technique for measuring the thermal conductivities of a wide range of materials. Utilizing nonlinear data enhances the determination of multiple thermophysical properties at the micro- and nanoscales. However, challenges such as dependence on initial guesses and convergence to local minima render nonlinear fitting processes unstable. This study introduces a machine learning-based approach that addresses these limitations by pre-learning a globally optimal solution. We developed a methodology that processes three-omega signals using machine learning to determine various thermophysical properties. The approach involved compiling results from the analytical three-omega model and augmenting them with Gaussian noise to create a robust machine learning model. Subsequently, a neural network was trained on this dataset. Testing confirmed the model's accurate predictions of volumetric heat capacity and thermal conductivity. Comparative analyses between machine learning-based and conventional fitting methods on the sample data extracted from the test set demonstrated the superior stability of the machine learning model in predicting thermophysical properties. Furthermore, experimental validation was carried out by applying our machine learning model to real-world data from glass and liquid samples. The correspondence between the predicted values and the theoretical curve of the third harmonic voltage affirmed the model's applicability and accuracy in practical scenarios. These findings validate the potential of our machine learning model for robustly predicting thermophysical properties based on actual measured data.

The heat generation density associated with the miniaturization of semiconductor devices has emerged as a critical issue in recent years,[1,2] emphasizing the increasingly vital role of materials' thermophysical properties in enhancing device performance. Significant advancements have been made in measurement techniques for these properties, including the transient hotwire technique,[3,4] Raman spectroscopy,[5,6] thermoreflectance method,[7,8] laser flash method,[9] and the three-omega method.[10] The three-omega method is recognized for its simplicity and precision and measures the thermophysical properties of a diverse array of materials, including bulk materials,[10–13] thin films,[14–16] gases,[17–19] liquids,[20–23] and soft materials.[13,15,24] This technique involves passing an alternating current with an angular frequency (1ω) through a metal line heater, generating a third harmonic voltage ($V_{3\omega}$) due to the resistance changes induced by temperature variations.

Our measurements focused on the third harmonic voltage to determine the material's thermophysical properties. In the low-frequency region, the relationship between the third harmonic voltage and frequency is linear, simplifying the estimation of a sample's thermal conductivity. However, for accurate measurements of micro- and nanoscale materials, nonlinear fitting-based analysis is indispensable in higher frequency regions.[22] Additionally, the determination of multiple thermophysical properties, such as volumetric heat capacity or thermal boundary conductance, necessitates the use of nonlinear fitting.[11,22] Despite its utility, nonlinear fitting poses challenges; it is time-intensive

and prone to instability, often leading to errors due to convergence to suboptimal solutions and dependence on initial guesses.

Employing a machine learning method to process measured data presents a robust solution to prevailing challenges, as it is capable of learning globally optimal solutions in advance. Extensive literature reviews and studies have explored the application of machine learning for data processing and property prediction in thermal engineering.[25–27] For instance, deep learning techniques have been instrumental in estimating thermophysical properties, thereby enhancing our understanding of related phenomena.[28–31] Moreover, deep learning-based techniques have been integrated into various measurement methods,[32–35] particularly enriching the analysis capabilities within the field of thermoreflectance.[36–39] Despite these advancements, the application of machine learning methodologies to three-omega measurements remains underexplored, indicating a significant area for further research.

In this study, a machine learning-based analytical approach was designed for the three-omega method to ensure stable analysis. We constructed machine learning models, specifically neural networks, to predict the thermophysical properties of materials. An analytical database, augmented with Gaussian noise, was employed to train these models. The effectiveness of our machine learning models was corroborated through both analytical and experimental data.

In the analytical phase, a test set derived from the analytical database was utilized to evaluate the precision of the machine learning models' predictions. Comparisons between conventional fitting analyses and machine learning predictions on the test set data demonstrated that machine learning offers more accurate and stable results. Additionally, we analyzed experimentally measured data from solid and liquid samples, confirming the accuracy of the predictions and the overall effectiveness of the machine learning analysis method.

In the three-omega method, an alternating current $(I_0 \cos \omega t)$ with an angular frequency (1ω) passes through a metal wire heater placed on a substrate, inducing Joule heating that oscillates at a frequency of $2\,\omega$. This heating causes the temperature rise of the heater (ΔT) to oscillate at 2ω, which in turn causes the resistance of the heater $(R_0 + \Delta R)$ to oscillate at the same frequency. The oscillating resistance, combined with the alternating current, produces a heater voltage component at $3\,\omega$, as described by the following equation:

$$V_{3\omega} = \frac{R_0 I_0 \beta}{2} \Delta T, \tag{1}$$

where β represents the temperature coefficient of resistance. Here, note that ΔT, ΔR, and $V_{3\omega}$ are complex amplitudes.

The temperature rise in the heater is influenced by the structure and thermophysical properties of the surrounding materials and is theoretically determined using the heat conduction equation.[12,14,40,41] In a configuration where multiple material layers are arranged in parallel, the temperature rise can be expressed as follows:

$$\Delta T = \frac{P}{2l\pi} \int_0^\infty \frac{\sin^2(mb)}{(mb)^2 k_j \sqrt{m^2 + q_j^2}} \times \frac{B^+ + B^-}{A^+ B^- - A^- B^+} dm, \tag{2}$$

where P, l, and $2b\,(l \gg b)$ represent the heating power, length, and width of the heater, respectively.[16] q_i denotes the wavenumber in layer i, defined as $q_i = \sqrt{\frac{i2\omega C_i}{k_i}}$, where k_i denotes thermal conductivity and C_i denotes volumetric heat capacity. The subscript j represents the layer in which the heater is located. In addition, A^+, A^-, B^+, and B^- are the elements of complex matrices $\boldsymbol{A}$ and $\boldsymbol{B}$ in the matrix formalism.[41]

We assume the simplest system consists of an air layer and a sample layer, as depicted in Fig. 1(a), treating both as semi-infinite in the analytical model. The heater is positioned at the interface on the sample layer, with the volumetric heat capacity assumed to be negligible. The system is also assumed to be infinite in the length direction of the heater, and heat conduction is treated as two-dimensional. To evaluate the effectiveness of machine learning model, we constructed a metal line heater on a glass substrate as depicted in Fig. 1(b). In both analytical simulations and experimental setups, the in-phase component of the third harmonic voltage was employed to estimate the thermophysical properties, as this component typically provides more reliable data in the three-omega method.[10]

The construction of a machine learning-based data processing system for the three-omega method is outlined in Fig. 1(c). Initially, a theoretical database of third harmonic voltage is generated using the heat conduction model. This database is then segmented into training, validation, and test sets, with respective proportions of 72.25%, 12.75%, and 15%. The machine learning algorithm is trained using the training set, evaluated using the validation set, and the best-performing model during validation is subsequently tested with the test set. It is important to note that the training process relies exclusively on the synthetic database. A detailed discussion of the implications of this approach is provided in Sec. 1 of the supplementary material.

Using Eqs. (1) and (2), the third harmonic voltage is represented by a product of an integral term, $\int_0^\infty \frac{\sin^2(mb)}{(mb)^2 k_j \sqrt{m^2+q_j^2}} \times \frac{B^+ + B^-}{A^+ B^- - A^- B^+} dm$, and a constat term, $\frac{R_0 I_0 \beta P}{4l\pi}$, as shown below

$$V_{3\omega} = \frac{R_0 I_0 \beta P}{4l\pi} \int_0^\infty \frac{\sin^2(mb)}{(mb)^2 k_j \sqrt{m^2 + q_j^2}} \times \frac{B^+ + B^-}{A^+ B^- - A^- B^+} dm. \tag{3}$$

The parameters not involved in the integral term, such as the temperature coefficient of resistance (β), heater length (l), heater thickness (t_{heater}), electrical resistivity (ρ), and current value (I_0), were fixed, as shown in Fig. 1(c). When experimental data are inputted into the machine learning model, these data are scaled by the fixed parameters and experimental values to conform to the computational conditions of the database, as detailed in Sec. 2 of the supplementary material. Conversely, parameters related to the integral term are treated as inputs to the machine learning model due to the unpredictable effects their variations can have on the signal.

In this model, the inputs for the machine learning algorithm included the third harmonic voltage $(V_{3\omega})$ and half of the heater width (b), as shown in Fig. 1(c). The alternating current frequencies were uniformly set across 100 points on a logarithmic scale, ranging from 1 to 10 000 Hz. The machine learning model outputs were the sample volumetric heat capacity (C_{sample}) and thermal conductivity (k_{sample}). The thermophysical properties of air and other constant parameters are detailed in Table SI of the supplementary material. To construct the machine learning database, 500 000 data points were generated under these specified conditions, with Gaussian noise added to enhance model robustness. The noise levels were set such that the

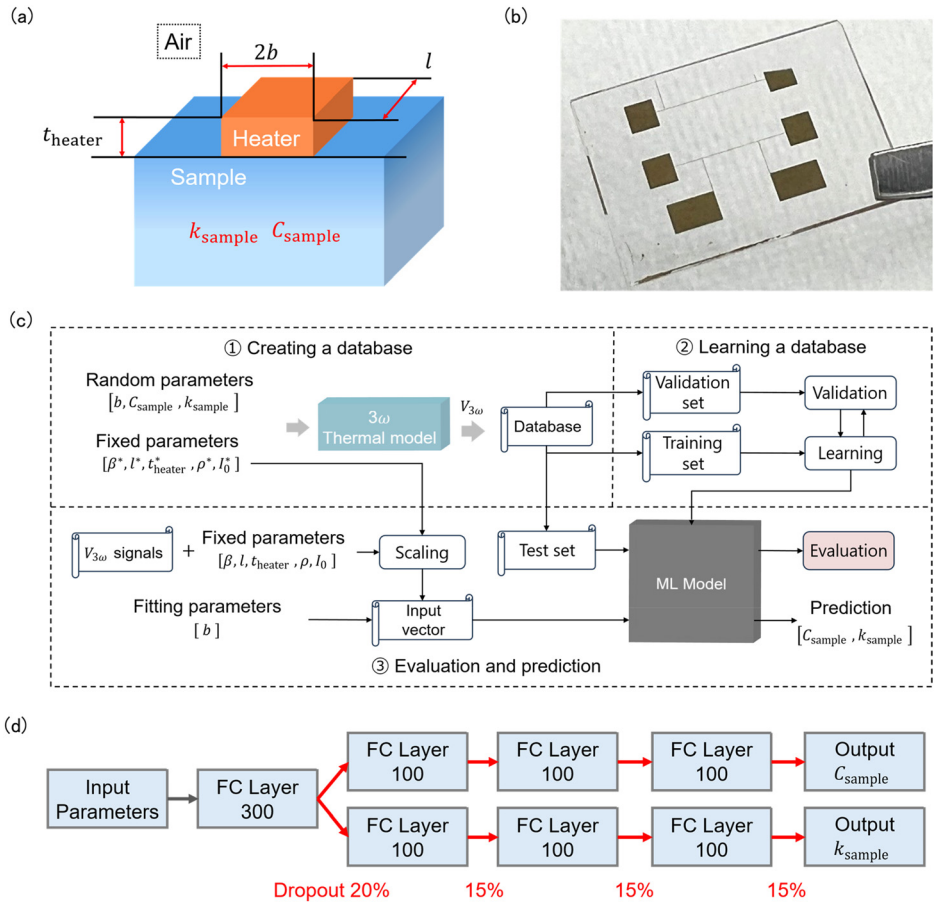

FIG. 1. (a) Configuration of the three-omega sample, consisting of two layers: an air layer and a sample layer, with a gold heater. (b) Example of samples used for experimental validation. (c) Workflow for constructing the machine learning (ML) model and performing validation. Parameters marked with an asterisk indicate fixed values used in database generation. (d) Architecture of the neural network, consisting of fully connected (FC) layers. The dropout of neurons is illustrated with red arrows, and the corresponding dropout rates are labeled.

standard deviation of the third harmonic voltage was 0.5% of the signal at 1 Hz, and for other input parameters, the standard deviation was maintained at 0.2%.

A neural network was employed due to its simplicity and strong representational capacity. To reduce overfitting, dropout[42,43] was applied, specifically using the Monte Carlo dropout method,[43] which involved 1000 stochastic forward passes with dropout enabled. The mean and standard deviation of these predictions were used as the final output and its associated uncertainty, respectively. The network architecture, shown in Fig. 1(d), utilizes exponential linear unit (ELU) activation.[44] Training was conducted using the root mean squared percentage error (RMSPE) as the loss function, along with the Adam optimizer.[45] Detailed information regarding the model architecture and training procedure is provided in Sec. 3 of the supplementary material.

The performance of the machine learning model was rigorously assessed using the test set. Evaluation metrics included the mean absolute percentage error (MAPE) and the coefficient of determination R^2, defined as follows:

$$\mathrm{MAPE} = \frac{100}{n}\sum_{i=1}^{n}\left|\frac{h(\boldsymbol{X}_i) - \boldsymbol{Y}_i}{\boldsymbol{Y}_i}\right|, \tag{4}$$

$$R^2 = 1 - \frac{\sum_{i=1}^{n}\left(h(\boldsymbol{X}_i) - \boldsymbol{Y}_i\right)^2}{\sum_{i=1}^{n}\left(\boldsymbol{Y}_i - \bar{\boldsymbol{Y}}\right)^2}, \tag{5}$$

where h represents the output of the machine learning model, $\boldsymbol{X}_i$, $\boldsymbol{Y}_i$ $(1 \le i \le n)$ denote the ith input and label data, respectively, and $\bar{\boldsymbol{Y}}$ is the average of the label data.

Table I presents the results of evaluating the predictions and statistical analysis of prediction uncertainty percentages for sample volumetric heat capacity and thermal conductivity using the trained machine learning model. The predicted values compared to the true values are displayed in Figs. 2(a) and 2(b), respectively, for volumetric heat capacity and thermal conductivity. According to Table I, the MAPE for both volumetric heat capacity and thermal conductivity was below 3%. Moreover, Figs. 2(a) and 2(b) demonstrate that the prediction error is less than 10% in most cases, confirming the model's capability to accurately predict the thermophysical properties.

TABLE I. Evaluation and prediction uncertainty of sample volumetric heat capacity (C_{sample}) and thermal conductivity (k_{sample}).

	Evaluation		Uncertainty %	
Parameter	R^2	MAPE %	Mean	Standard deviation
C_{sample}	0.9919	2.375	5.820	1.116
k_{sample}	0.9985	1.313	7.342	0.983

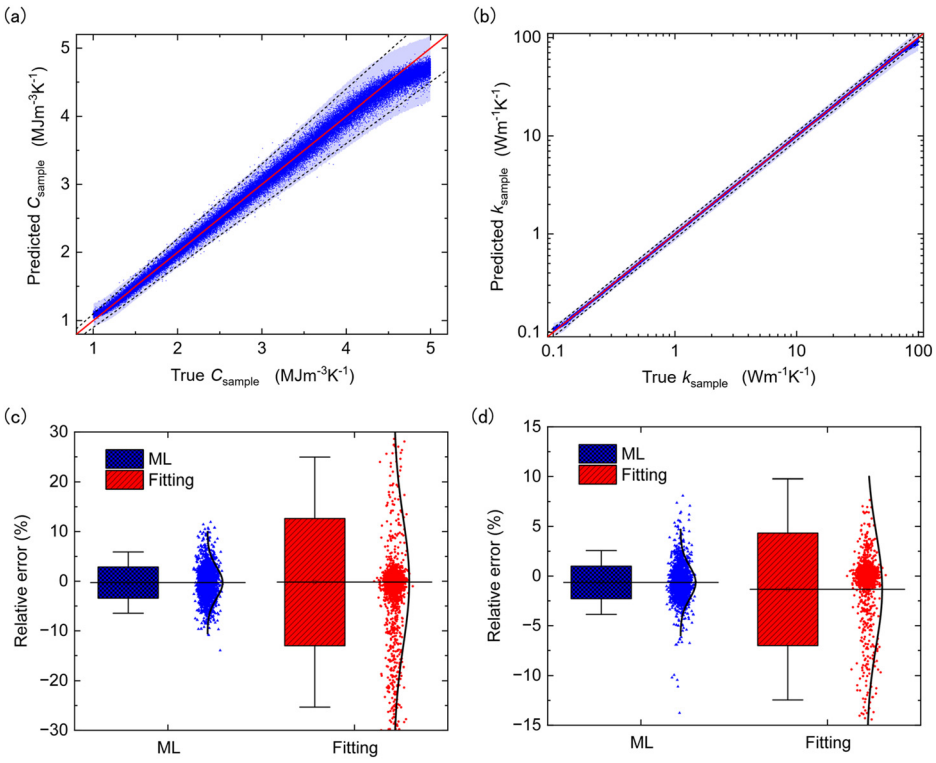

FIG. 2. Predictions from the ML model: (a) Volumetric heat capacity (C_{sample}) and (b) thermal conductivity (k_{sample}) of the sample. Accuracy is indicated when data points are near the solid red line. Black dashed lines represent the ± 10% error. Blue shaded regions denote the 95% confidence intervals around the mean predictions. Panels (c) and (d) compare percentage errors in C_{sample} and k_{sample} between our machine learning model and conventional fitting methods. The box plots show the range within one standard deviation, with whiskers extending to the 95% confidence intervals. Individual data and corresponding normal distribution curves are displayed beside each box.

Additionally, we conducted a comparative analysis between the predictions made by our machine learning model and those derived from a conventional fitting algorithm. The comparison utilized a dataset comprising 2000 randomly sampled data points from the test set. The fitting parameters are the volumetric heat capacity (C_{sample}) and thermal conductivity of the sample (k_{sample}). Both methods were evaluated based on the relative error between the obtained and true values, allowing for a direct comparison of predictive accuracy.

Figures 2(c) and 2(d) depict the plot and distribution of the relative error for each data point in the target dataset pertaining to the volumetric heat capacity and thermal conductivity of the sample, respectively. Table II provides a statistical overview of the relative errors for predictions made using both the machine learning model and the fitting algorithm. The predictions from the fitting algorithm can deviate significantly from the true values, as evidenced in Figs. 2(c) and 2(d). Consequently, the standard deviation, MAPE, and maximum absolute percentage error of the relative errors from our machine learning model are lower than those from the fitting algorithm for each thermophysical property. This difference can be attributed to the robustness of the machine learning-based analysis and the inherent instability of the fitting process, including its sensitivity to initial guesses and its tendency to converge to local minima. Details of the fitting procedure, along with additional simulations supporting this approach, are provided in Sec. 4 of the supplementary material.

TABLE II. Statistics of relative error for predicting sample volumetric heat capacity (C_{sample}) and thermal conductivity (k_{sample}) by machine learning (ML) and fitting algorithm, expressed in percentages.

	C_{sample}		k_{sample}	
	ML	Fitting	ML	Fitting
Mean of percentage error	−0.28	−0.184	−0.648	−1.338
MAPE	2.421	5.678	1.317	2.090
Standard deviation of relative error	3.145	12.82	1.642	5.670
Max absolute percentage error	13.95	95.18	13.77	40.99

Moreover, the effectiveness of our machine learning models was further validated through the processing of actual experimental data. We conducted measurements on the third harmonic voltage from a sample composed of glass and a gold line heater, with a corresponding photograph displayed in Fig. 1(b). The experimental setup is the same as our previous work.[23] By integrating these data into the process outlined in Fig. 1(c) and applying it to our machine learning model, we were able to predict the volumetric heat capacity and thermal conductivity of the sample. The parameters used for the fitting are detailed in Table SIII of the supplementary material.

Figure 3 presents the third harmonic voltage measurements obtained from our experimental setup alongside the theoretical curves derived from the parameters predicted by both the machine learning model and the fitting algorithm. The predicted values for the volumetric heat capacity and thermal conductivity are enumerated in Table III. As demonstrated in Fig. 3, the theoretical curve based on predictions from the machine learning model aligns closely with the experimental data, affirming the model's applicability to real-world data.

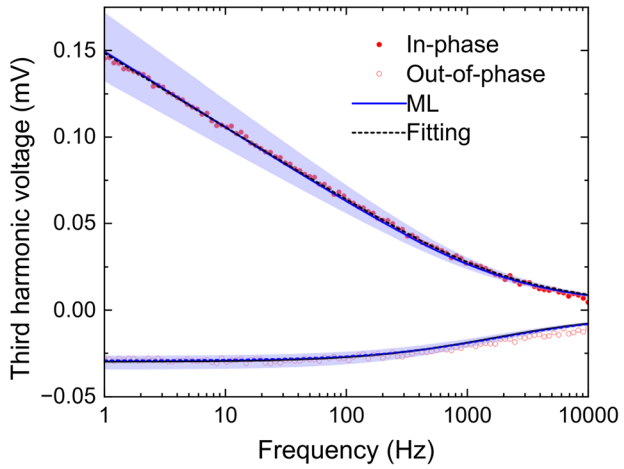

FIG. 3. Experimental signals of the third harmonic voltage. Filled markers represent in-phase component, and unfilled markers represent the out-of-phase component. The solid blue line represents the thermal model predictions based on the outputs from the ML model, while the dashed black line represents the fitting predictions. The shaded region around the solid blue line indicates the 95% confidence interval derived from prediction uncertainty.

TABLE III. Predicted results for sample volumetric heat capacity (C_{sample}) and thermal conductivity (k_{sample}) by ML model and fitting algorithm.

	ML	Fitting
C_{sample} (MJ m^{-3} K^{-1})	2.136±0.122	1.890
k_{sample} (W m^{-1} K^{-1})	1.214±0.083	1.247

The predicted values for volumetric heat capacity from the machine learning and fitting algorithms exhibited an error of approximately 10%. This variation may stem from the relatively low sensitivity of volumetric heat capacity measurements. This assertion is supported by the greater variation in predictions for volumetric heat capacity compared to thermal conductivity, as detailed in Table II. Additionally, deviations in the out-of-phase component from the theoretical model were particularly noticeable in high-frequency regions. Such deviations are likely influenced by experimental noise and the precision of the heat conduction model employed to develop the machine learning database. To explore the implications of incorporating out-of-phase components in machine learning models, a detailed discussion is provided in Sec. 6 of the supplementary material.

Furthermore, the effectiveness of the machine learning methodology was also confirmed through measurements on liquid samples using a three-omega sensor based on a parylene substrate, recently developed by our research group.[23] Figure 4(a) depicts the system configuration, which includes three layers: an air layer, a parylene substrate layer, and a sample layer. Figure 4(b) presents an example of a parylene-substrate three-omega sensor. In this setup, it is assumed that thermal boundary resistance exists between the parylene substrate and the sample layers, adding another layer of complexity to the thermal measurements.

In this study, a machine learning model was designed to predict the thermal conductivity of a sample and the thermal boundary conductance between the parylene substrate and the sample layers. Notably, the inputs for the model included the thickness of the parylene substrate ($t_{parylene}$), the sample's volumetric heat capacity (C_{sample}), and half of the heater width (b). The outputs were the sample's thermal conductivity (k_{sample}) and thermal boundary conductance (G). The parameter ranges, including the thermal conductivity ($k_{parylene}$) and volumetric heat capacity of the parylene ($C_{parylene}$), and further details about the architecture of this model and its evaluation on the test set can be found in Sec. 7 of the supplementary material.

The trained model was subsequently applied to experimental data from a previous study[23] on water, isopropyl alcohol (IPA), and their mixtures, as shown in Fig. 5(a). Along with theoretical predictions for thermal conductivity, the predicted values for the sample's thermal conductivity and thermal boundary conductance are shown in Fig. 5(b), and the specific values are listed in Table IV. The theoretical predictions are based on mixing theory.[46] As shown in Fig. 5(b), errors in the predicted thermal conductivity values compared to the theoretical values were less than 15%. Additionally, the predicted thermal boundary conductance showed an increase with a higher water volume fraction. However, given that parylene substrates are hydrophobic, and IPA exhibits better wettability to these substrates than water,[47,48] the interpretation of wettability as a factor in thermal boundary conductance is inconsistent with these predictions and warrants further exploration.

This study presented a machine learning-based analytical framework for the three-omega method. An analytical dataset was

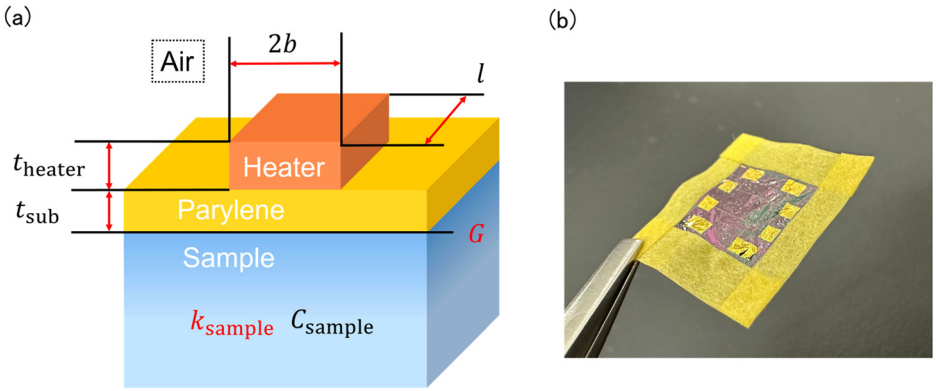

FIG. 4. (a) System configuration of the three-omega sample using a parylene substrate. The system comprises three layers: an air layer, a parylene substrate layer, and a sample layer, with a gold heater integrated. (b) An example of a three-omega sensor based on a parylene substrate.

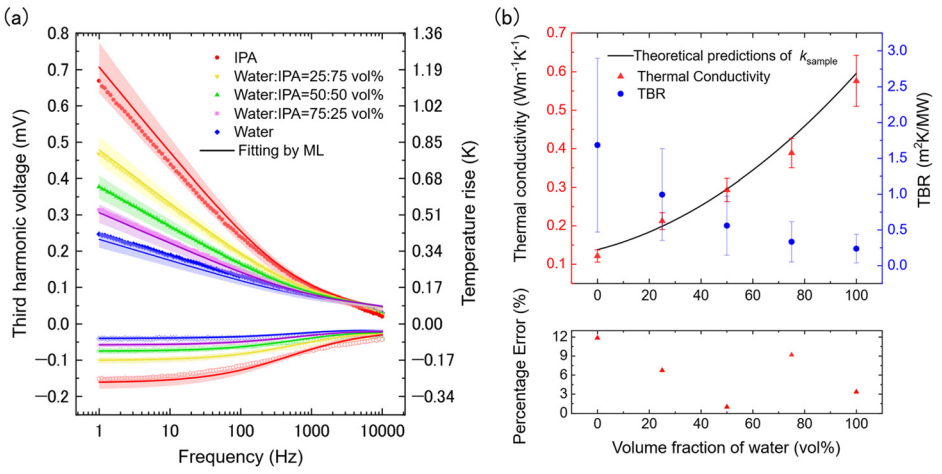

FIG. 5. Validation of predictions using an experimental dataset of water, IPA, and their mixtures. (a) Third harmonic voltage: filled markers indicate the in-phase component, and unfilled markers the out-of-phase component. Solid lines represent thermal model predictions derived from ML model outputs, with shaded regions denoting the 95% confidence intervals. (b) The upper graph shows predicted thermal conductivity (k_{sample}) and thermal boundary resistance (TBR, $1/G$) vs water volume fraction, with theoretical predictions. The lower graph shows the absolute percentage errors of the predicted thermal conductivity compared with theoretical values.

TABLE IV. Theoretical and predicted values of thermal conductivity, along with prediction uncertainties for thermal boundary conductance and thermal conductivity for the experimental dataset comprising water, isopropyl alcohol (IPA), and their mixtures.

Volume fraction of water (vol. %)		0 %	25 %	50 %	75 %	100 %
k_{sample} (W m^{-1} K^{-1})	Theoretical value	0.138	0.199	0.296	0.428	0.596
	ML Prediction	0.122	0.213	0.293	0.388	0.576
	Uncertainty	0.008	0.011	0.015	0.019	0.033
G (M Wm^{-2} K^{-1})	ML Prediction	0.594	1.006	1.786	2.997	4.209
	Uncertainty	0.214	0.324	0.660	1.263	1.783

constructed, and neural network models were developed to predict the thermophysical properties of various samples. Model accuracy was evaluated using a designated test set from the analytical database. In comparison with conventional fitting techniques, the machine learning approach exhibited reduced variability and enhanced robustness. Application to experimental data further confirmed the reliability of the model's predictions, thereby demonstrating the practical effectiveness of the proposed method. We validated the approach by analyzing experimental data obtained from measurements on water, IPA, and their mixtures. These findings suggest that our methodology is adaptable to other systems employing the three-omega method, and we anticipate further developments and applications of this technique in the future.

See the supplementary material for detailed information about our machine learning methodology and results.

This work was financially supported by the JST PRESTO (JPMJPR20B6), multiple JSPS Grants-in-Aid for Scientific Research (19H02168, 20KK0087, 23K04361, 23K26139, and 24K21577), and a JSPS Grant-in-Aid for JSPS Fellows (24KJ1526). Computational resources were provided by the ACCMS, Kyoto University. This work partly used computational resources of the supercomputer Fugaku provided by RIKEN through the HPCI System Research Project (Project ID: hp240303). Additionally, this project was partly supported by the Kyoto University Nanotechnology Hub as part of the "Advanced Research Infrastructure for Materials and Nanotechnology Project," which is funded by the Ministry of Education, Culture, Sports, Science and Technology (MEXT), Japan.

AUTHOR DECLARATIONS

Conflict of Interest

The authors have no conflicts to disclose.

Author Contributions

Yasuaki Ikeda: Conceptualization (lead); Data curation (lead); Formal analysis (lead); Methodology (lead); Resources (lead); Software (lead); Visualization (lead); Writing – original draft (lead). **Yuki Akura:** Formal analysis (supporting); Methodology (supporting); Software (supporting); Writing – review & editing (supporting). **Ryuto Yamasaki:** Conceptualization (supporting); Formal analysis (supporting); Methodology (supporting); Resources (equal); Software (supporting). **Yuki Matsunaga:** Formal analysis (supporting); Methodology (supporting); Resources (equal). **Lijun Liu:** Conceptualization (supporting); Formal analysis (supporting); Writing – review & editing (supporting). **Masaki Shimofuri:** Conceptualization (supporting); Writing – review & editing (supporting). **Amit Banerjee:** Conceptualization (supporting); Writing – review & editing (supporting). **Toshiyuki Tsuchiya:** Conceptualization (supporting); Project administration (supporting); Writing – review & editing (supporting). **Jun Hirotani:** Conceptualization (lead); Funding acquisition (lead);

Methodology (lead); Project administration (lead); Supervision (lead); Writing – review & editing (lead).

DATA AVAILABILITY

The data that support the findings of this study are available from the corresponding author upon reasonable request.

REFERENCES

[1]J. Baek, Y. Elasser, K. Radhakrishnan, H. Gan, J. P. Douglas, H. K. Krishnamurthy, X. Li, S. Jiang, C. R. Sullivan, and M. Chen, "Vertical stacked LEGO-PoL CPU voltage regulator," IEEE Trans. Power Electron. **37**(6), 6305–6322 (2022).

[2]M. Mehrvand and S. A. Putnam, "Probing the local heat transfer coefficient of water-cooled microchannels using time-domain thermoreflectance," J. Heat Transfer **139**(11), 112403 (2017).

[3]Y. Nagasaka and A. Nagashima, "Simultaneous measurement of the thermal conductivity and the thermal diffusivity of liquids by the transient hot-wire method," Rev. Sci. Instrum. **52**(2), 229–232 (1981).

[4]M. J. Assael, K. D. Antoniadis, D. Velliadou, and W. A. Wakeham, "Correct use of the transient hot-wire technique for thermal conductivity measurements on fluids," Int. J. Thermophys. **44**(6), 85 (2023).

[5]J. Anaya, S. Rossi, M. Alomari, E. Kohn, L. Tóth, B. Pécz, and M. Kuball, "Thermal conductivity of ultrathin nano-crystalline diamond films determined by Raman thermography assisted by silicon nanowires," Appl. Phys. Lett. **106**(22), 223101 (2015).

[6]H. Malekpour and A. A. Balandin, "Raman-based technique for measuring thermal conductivity of graphene and related materials," J. Raman Spectrosc. **49**(1), 106–120 (2018).

[7]A. J. Schmidt, R. Cheaito, and M. Chiesa, "A frequency-domain thermoreflectance method for the characterization of thermal properties," Rev. Sci. Instrum. **80**(9), 094901 (2009).

[8]D. G. Cahill, "Analysis of heat flow in layered structures for time-domain thermoreflectance," Rev. Sci. Instrum. **75**(12), 5119–5122 (2004).

[9]Y. Tada, M. Harada, M. Tanigaki, and W. Eguchi, "Laser flash method for measuring thermal conductivity of liquids—application to low thermal conductivity liquids," Rev. Sci. Instrum. **49**(9), 1305–1314 (1978).

[10]D. G. Cahill, "Thermal conductivity measurement from 30 to 750 K: The 3ω method," Rev. Sci. Instrum. **61**(2), 802–808 (1990).

[11]I. K. Moon, Y. H. Jeong, and S. I. Kwun, "The 3ω technique for measuring dynamic specific heat and thermal conductivity of a liquid or solid," Rev. Sci. Instrum. **67**(1), 29–35 (1996).

[12]B. W. Olson, S. Graham, and K. Chen, "A practical extension of the 3ω method to multilayer structures," Rev. Sci. Instrum. **76**(5), 053901 (2005).

[13]G. Boussatour, P. Y. Cresson, B. Genestie, N. Joly, J. F. Brun, and T. Lasri, "Measurement of the thermal conductivity of flexible biosourced polymers using the 3-omega method," Polym. Test. **70**, 503–510 (2018).

[14]J. H. Kim, A. Feldman, and D. Novotny, "Application of the three omega thermal conductivity measurement method to a film on a substrate of finite thickness," J. Appl. Phys. **86**(7), 3959–3963 (1999).

[15]J. Jin, M. P. Manoharan, Q. Wang, and M. A. Haque, "In-plane thermal conductivity of nanoscale polyaniline thin films," Appl. Phys. Lett. **95**(3), 033113 (2009).

[16]R. E. Bernhardsgrütter, C. J. Hepp, K. Schmitt, M. Jägle, H.-F. Pernau, and J. Wöllenstein, "Towards a robust thin film sensor for distinguishing fluids using the 3ω method," Sens. Actuators, A **321**, 112419 (2021).

[17]E. Yusibani, P. L. Woodfield, M. Kohno, K. Shinzato, Y. Takata, and M. Fujii, "End effects in the three-omega method to measure gas thermal conductivity," Int. J. Thermophys. **30**(3), 833–850 (2009).

[18]E. Yusibani, P. L. Woodfield, S. Moroe, K. Shinzato, M. Kohno, Y. Takata, and M. Fujii, "A procedure for application of the three-omega method to measurement of gas thermal conductivity," J. Therm. Sci. Technol. **4**(1), 146–158 (2009).

[19]S. Gauthier, A. Giani, and P. Combette, "Gas thermal conductivity measurement using the three-omega method," Sens. Actuators, A **195**, 50–55 (2013).

[20]S. R. Choi, J. Kim, and D. Kim, "3ω method to measure thermal properties of electrically conducting small-volume liquid," Rev. Sci. Instrum. **78**(8), 084902 (2007).

[21]Z. L. Wang, D. W. Tang, S. Liu, X. H. Zheng, and N. Araki, "Thermal-conductivity and thermal-diffusivity measurements of nanofluids by 3ω method and mechanism analysis of heat transport," Int. J. Thermophys. **28**(4), 1255–1268 (2007).

[22]S. Roy-Panzer, T. Kodama, S. Lingamneni, M. A. Panzer, M. Asheghi, and K. E. Goodson, "Thermal characterization and analysis of microliter liquid volumes using the three-omega method," Rev. Sci. Instrum. **86**(2), 024901 (2015).

[23]R. Yamasaki, Y. Matsunaga, Y. Akura, M. Shimofuri, A. Banerjee, T. Tsuchiya, and J. Hirotani, "Flexible 3ω sensors on submicron-thick parylene substrates for thermal conductivity measurements of liquids and soft materials," Appl. Phys. Lett. **126**(1), 014101 (2025).

[24]S. D. Lubner, J. Choi, G. Wehmeyer, B. Waag, V. Mishra, H. Natesan, J. C. Bischof, and C. Dames, "Reusable bi-directional 3ω sensor to measure thermal conductivity of 100-μm thick biological tissues," Rev. Sci. Instrum. **86**(1), 014905 (2015).

[25]R. Guo, B.-Y. Cao, T. Luo, and A. J. H. McGaughey, "Machine learning for thermal transport," J. Appl. Phys. **136**(16), 160401 (2024).

[26]X. Huang and S. Ju, "Tutorial: AI-assisted exploration and active design of polymers with high intrinsic thermal conductivity," J. Appl. Phys. **135**(17), 171101 (2024).

[27]Y. Hu, Q. Wang, and H. Ma, "Machine-learning-assisted searching for thermally conductive polymers: A mini review," J. Appl. Phys. **135**(12), 120701 (2024).

[28]T. Zhan, L. Fang, and Y. Xu, "Prediction of thermal boundary resistance by the machine learning method," Sci. Rep. **7**(1), 7109 (2017).

[29]Y.-J. Wu, T. Zhan, Z. Hou, L. Fang, and Y. Xu, "Physical and chemical descriptors for predicting interfacial thermal resistance," Sci. Data **7**(1), 36 (2020).

[30]Y. Srivastava and A. Jain, "End-to-end material thermal conductivity prediction through machine learning," J. Appl. Phys. **134**(22), 225101 (2023).

[31]C. Zhu, T. Luo, B. Li, X. Shen, and G. Zhu, "Machine learning aided understanding and manipulating thermal transport in amorphous networks," J. Appl. Phys. **135**(19), 195103 (2024).

[32]S. Sripada, A. U. Gaitonde, J. A. Weibel, and A. M. Marconnet, "Robust inverse parameter fitting of thermal properties from the laser-based Ångstrom method in the presence of measurement noise using physics-informed neural networks (PINNs)," J. Appl. Phys. **135**(22), 225106 (2024).

[33]C. Dunlap, C. Li, H. Pandey, N. Le, and H. Hu, "BubbleID: A deep learning framework for bubble interface dynamics analysis," J. Appl. Phys. **136**(1), 014902 (2024).

[34]H. Cao, B. Kwon, and P. K. Kang, "Inferring temperature fields from concentration fields in channel flows using conditional generative adversarial networks," J. Appl. Phys. **135**(21), 214701 (2024).

[35]M. Ali Boroumand, G. Morra, and P. Mora, "Extracting fundamental parameters of 2D natural thermal convection using convolutional neural networks," J. Appl. Phys. **135**(14), 144702 (2024).

[36]Y. Pang, P. Jiang, and R. Yang, "Machine learning-based data processing technique for time-domain thermoreflectance (TDTR) measurements," J. Appl. Phys. **130**(8), 084901 (2021).

[37]W. Shen, D. Vaca, and S. Kumar, "Reconsidering uncertainty from frequency domain thermoreflectance measurement and novel data analysis by deep learning," Nanoscale Microscale Thermophys. Eng. **24**(3–4), 138–149 (2020).

[38]A. Jarzembski, Z. T. Piontkowski, W. Hodges, M. Bahr, A. McDonald, W. Delmas, G. W. Pickrell, and L. Yates, "Rapid subsurface analysis of frequency-domain thermoreflectance images with K-means clustering," J. Appl. Phys. **135**(16), 165102 (2024).

[39]Y. Ikeda, Y. Akura, M. Shimofuri, A. Banerjee, T. Tsuchiya, and J. Hirotani, "Estimating depth-directional thermal conductivity profiles using neural network with dropout in frequency-domain thermoreflectance," J. Appl. Phys. **137**(5), 055106 (2025).

[40]T. Borca-Tasciuc, A. R. Kumar, and G. Chen, "Data reduction in 3ω method for thin-film thermal conductivity determination," Rev. Sci. Instrum. **72**(4), 2139–2147 (2001).

[41]A. Feldman, "Algorithm for solutions of the thermal diffusion equation in a stratified medium with a modulated heating source," High Temp–High. Press. **31**(3), 293–298 (1999).

[42]N. Srivastava, G. Hinton, A. Krizhevsky, I. Sutskever, and R. Salakhutdinov, "Dropout: A simple way to prevent neural networks from overfitting," J. Mach. Learn. Res. **15**(56), 1929–1958 (2015).
[43]Y. Gal and Z. Ghahramani, "Dropout as a Bayesian approximation: representing model uncertainty in deep learning," in Proceedings of the 33rd International Conference on International Conference on Machine Learning, 2016.
[44]D.-A. Clevert, T. Unterthiner, and S. Hochreiter, "Fast accurate deep network learn by Exponential Linear Units (ELUs)," arXiv:1511.07289 [cs.LG] (2016).
[45]D. P. Kingma and J. Ba, "Adam: A method for stochastic optimization," arXiv:1412.6980 [cs.LG] (2017).
[46]C. C. Li, "Thermal conductivity of liquid mixtures," AIChE J. **22**(5), 927–930 (1976).
[47]M. Lundgren, N. L. Allan, T. Cosgrove, and N. George, "Wetting of water and water/ethanol droplets on a non-polar surface: A molecular dynamics study," Langmuir **18**(26), 10462–10466 (2002).
[48]A. K. Metya, S. Khan, and J. K. Singh, "Wetting transition of the ethanol–water droplet on smooth and textured surfaces," J. Phys. Chem. C **118**(8), 4113–4121 (2014).

Supplementary Material

"Utilizing machine learning in the three-omega method to predict thermophysical properties with low variation"

Yasuaki Ikeda[1], Yuki Akura[1], Ryuto Yamasaki[1], Yuki Matsunaga[2], Lijun Liu[3], Masaki Shimofuri[1], Amit Banerjee[1], Toshiyuki Tsuchiya[1], and Jun Hirotani[1] a)

[1]*Department of Micro Engineering, Graduate School of Engineering, Kyoto University, Kyotodaigaku-katsura, Nishikyo-ku, Kyoto 615-8540, Japan*

[2]*Department of Chemistry, Graduate School of Science, Nagoya University, Furo-cho, Chikusa-ku, Nagoya 464-8602, Japan*

[3]*Department of Mechanical Engineering, Graduate School of Engineering, Osaka University, 2-1 Yamadaoka, Suita, Osaka 565-0871, Japan*

Corresponding author

[a)]E-mail : hirotani.jun.7v@kyoto-u.ac.jp

1. Effect of synthetic dataset and noise

This section outlines the limitations of the proposed machine learning approach and discusses potential future directions. Our machine learning model is trained only on a synthetic dataset with added Gaussian noise. This strategy enables the generation of a large and diverse dataset, which enhances learning efficiency and improves predictive accuracy.

However, significant deviations from ideal signal conditions—such as those arising from systematic noise—must be addressed during the measurement process or through data preprocessing. Moreover, the analytical three-omega model does not fully capture the complexities of real experimental conditions. For instance, the model assumes negligible heat conduction within the heater, which may lead to inaccuracies when the heater's heat capacity is non-negligible.

To address these limitations, incorporating experimentally obtained data into the training dataset can improve the robustness and accuracy of the model. However, collecting a sufficiently large and diverse set of labeled experimental data for the three-omega method presents considerable challenges. The limited variability in such datasets may also introduce bias. As a potential future direction, transfer learning is under consideration.[1] In this approach, the model is initially trained on synthetic data and subsequently fine-tuned using a smaller set of experimental data, thereby combining the advantages of both data sources.

2. Scaling method for data preprocessing

As shown in Eq. (3) of the main text, the third harmonic voltage, $V_{3\omega}$, is expressed as the product of a constant term and an integral term:

$$V_{3\omega} = \frac{R_0 I_0 \beta P}{4l\pi} \int_0^{\infty} \frac{\sin^2(mb)}{(mb)^2 k_j \sqrt{m^2 + q_j^2}} \times \frac{B^+ + B^-}{A^+ B^- - A^- B^+} dm, \qquad (S1)$$

where $R_0, I_0, \beta, P, and\ l$ in the constant term represent the heater resistance, current amplitude, temperature coefficient of resistance, heating power, and heater length, respectively. These quantities influence the magnitude of the third harmonic voltage, and may vary between experiments due to differences in heater material and fabrication conditions. However, explicit inclusion of these parameters in the dataset can be avoided by applying an appropriate scaling method, as outlined below.

By incorporating the temperature coefficient of resistance (β), heater length (l), heater thickness (t_{heater}), electrical resistivity (ρ), and current amplitude (I_0), the constant term Z can be reformulated as:

$$Z = \frac{R_0 I_0 \beta P}{4l\pi} = \frac{R_0^2 I_0^3 \beta}{8l\pi} = \left(\rho \frac{l}{2bt_{\mathrm{heater}}}\right)^2 \frac{I_0^3 \beta}{8l\pi} = \frac{\rho^2 l I_0^3 \beta}{32 b^2 t_{\mathrm{heater}}^2 \pi}. \qquad (S2)$$

In constructing the database, the parameters $\beta, l, t_{\mathrm{heater}}, \rho$ and I_0 are treated as constants, and their fixed values are denoted with an asterisk (*). It should be noted that the half-width of the heater width (b) also appears in the integral term, and thus cannot be treated as a fixed parameter.

Given this, the ratio between the scaled constant Z^* (calculated using fixed parameters for database generation) and the actual value Z is expressed as:

$$\frac{Z^*}{Z} = \frac{\left(\frac{\rho^*}{\rho}\right)^2 \left(\frac{l^*}{l}\right) \left(\frac{I_0^*}{I_0}\right)^3 \left(\frac{\beta^*}{\beta}\right)}{\left(\frac{t_{\mathrm{heater}}^*}{t_{\mathrm{heater}}}\right)^2}. \qquad (S3)$$

Therefore, by multiplying the experimentally measured third harmonic voltage by this ratio, consistency with the database conditions can be maintained.

3. Architecture and training of our machine learning model

The neural network architecture consists of a shared fully connected (FC) layer with 300 units, followed by two parallel branches dedicated to predicting C_{sample} and k_{sample}, respectively. Each branch contains three FC layers with 100 units each, as depicted in Fig. 1(d) of the main text. To reduce overfitting, regularization was applied using the dropout method.[2,3]

For all activation functions within the neural network, an exponential linear unit (ELU) function[4] was employed, defined as:

$$f(x) = \begin{cases} x & (x > 0) \\ \alpha(\exp(x) - 1) & (x \leq 0) \end{cases}, \tag{S4}$$

where α is a hyperparameter typically set to 1, as was the case in this study. The root mean square percentage error (RMSPE) was selected as the training error function due to its sensitivity to outliers

$$\text{RMSPE} = 100 \sqrt{\frac{1}{n}\sum_{i=1}^{n}\left(\frac{h(\boldsymbol{X}_i) - \boldsymbol{Y}_i}{\boldsymbol{Y}_i}\right)^2}. \tag{S5}$$

Additionally, a relative-error-based index was adopted as the error function to accommodate a broad spectrum of thermal conductivities.

Initial weights were assigned using the He initialization scheme.[5] The network was trained for 200,000 epochs using RMSPE as the loss function. A batch size of 30,000 was employed, and optimization was performed using the Adam algorithm[6] with an initial learning rate of 10^{-5}, $\beta_1 = 0.99, \beta_2 = 0.999$, and $\epsilon = 10^{-7}$, deviating from default values only in the learning rate.

Model training was conducted on a workstation equipped with an NVIDIA RTX 4080 GPU, a 13th Gen Intel® Core™ i9-13900K CPU, and 64 GB of RAM. The software

environment included Python (version 3.10.10) and TensorFlow (version 2.14.0). Training required approximately 6 h to complete. Although hyperparameter optimization was not exhaustively performed—leaving open the possibility for further improvement—the model exhibited satisfactory performance and was therefore adopted for this study.

When compiling the machine learning database, each parameter was defined as detailed in Table SI. The thermophysical parameters for air were referenced from literature.[7]

TABLE SI. Physical parameters used in the database for our machine learning model.

	Parameter	Range	Units
Constant	C_{air}	1.167	$\mathrm{kJm^{-3}K^{-1}}$
	k_{air}	0.0263	$\mathrm{Wm^{-1}K^{-1}}$
Scaling	β^*	2200	ppm
	l^*	1	mm
	t^*_{heater}	100	nm
	ρ^*	2.35×10^{-8}	Ωm
	I^*_0	2	mA
Input	b	$5.0 - 15.0$	μm
Output	C_{sample}	$1.0 - 5.0$	$\mathrm{MJm^{-3}K^{-1}}$
	k_{sample}	$0.1 - 100$	$\mathrm{Wm^{-1}K^{-1}}$

4. Implementation of the fitting method and the fitting method with initial guess by machine learning model

In our research, the fitting process was performed using the "curve_fit" function from the SciPy package in Python. From the results of Section 6 in the Supplementary Material, only in-phase components were used in the data for fitting. In normal fitting, the initial values were fixed regardless of the data.

To confirm that the large deviations in the prediction result by the normal fitting method was due to its inherent instability, we also conducted a fitting analysis based on the initial guess by the machine learning model, in addition to the simulation results shown in Fig. 2(c), (d) in the main text. In this simulation, 2,000 data from the test set in two-layer model were analyzed by machine learning model, fitting method, and fitting method with initial guess by machine learning model. The results are shown in Fig. S1 and Table SII. The analysis results by the fitting method based on the initial guess of the machine learning model show lower relative error compared to the original fitting method and original machine learning method do.

These results indicate that the large deviations in the predictions obtained by the conventional fitting method can be attributed to its strong dependence on the initial guess. This dependence suggests that the optimization process is susceptible to convergence to local minima, leading to reduced accuracy. In contrast, the use of machine learning exhibits greater robustness against such issues, resulting in more stable and reliable predictions.

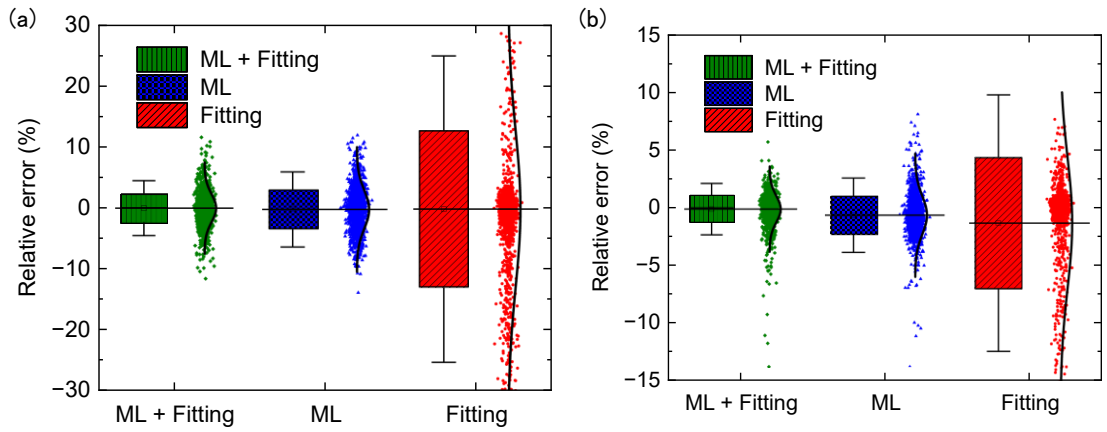

Figure S1. Comparative predictions for (a) volumetric heat capacity and (b) thermal conductivity of the sample obtained using the original machine learning model (ML), the original fitting method (Fitting), and the fitting method initialized with machine learning predictions (ML + Fitting). The box plots represent the range within one standard deviation, with whiskers extending to the 95% confidence intervals. Individual data points are plotted alongside a normal distribution curve.

TABLE SII. Relative error statistics (in %) for the different prediction methods.

	C_{sample}			k_{sample}		
	ML + Fitting	ML	Fitting	ML + Fitting	ML	Fitting
Mean of percentage error	−0.078	−0.280	−0.184	−0.109	−0.648	−1.338
MAPE	1.625	2.421	5.678	0.682	1.317	2.090
Standard deviation of relative error	2.281	3.145	12.82	1.130	1.642	5.670
Max absolute percentage error	11.57	13.95	95.18	13.76	13.77	40.99

5. Detail of fitting parameters in processing experimental data on glass

In the validation using actual measurements, the volumetric heat capacity and thermal conductivity of the sample were predicted using both our machine learning model and a fitting algorithm. Additional parameters involved in this process are detailed in Table SIII.

TABLE SIII. Parameters utilized for processing the experimental data.

	Parameter	Range	Units
Constant	C_{air}	1.167	$\mathrm{kJm^{-3}K^{-1}}$
	k_{air}	0.0263	$\mathrm{Wm^{-1}K^{-1}}$
Scaling	β	2108	ppm
	l	3	mm
	t_{heater}	100	nm
	R_0	46.1	Ω
	I_0	7.354	mA
Input	b	10.71	μm

6. Machine learning model based on both in-phase and out-of-phase components of the third harmonic voltage

For comparative analysis, one machine learning model was trained using both the in-phase and out-of-phase components as inputs, while another model was trained using only the in-phase component. The database and training conditions remained consistent across both models. Figures S2(a) and S2(b) display the predicted versus true values for the sample's volumetric heat capacity and thermal conductivity, respectively. Table SIV provides an evaluation of the prediction results for the test set.

The evaluation of the sample's thermal conductivity yielded nearly identical results between the model utilizing only in-phase components and the model including out-of-phase components. However, the predictions for the sample's volumetric heat capacity improved with the inclusion of the out-of-phase component. This enhancement can be attributed to the inherently low sensitivity of volumetric heat capacity measurements, which benefit from the additional information provided by the out-of-phase component.

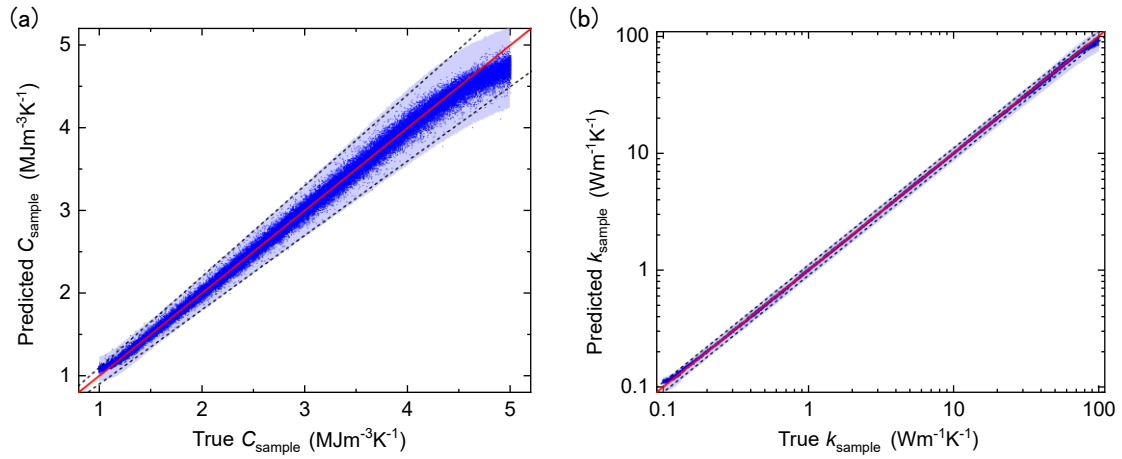

FIG. S2. Prediction results for the three-omega measurement system by the machine learning model using input with the out-of-phase component of the third harmonic voltage. Panel (a) shows the predictions for volumetric heat capacity (C_{sample}) and panel (b) for thermal conductivity (k_{sample}) of the sample. Accurate predictions are indicated when points are close to the solid red line. The black dashed lines denote the $\pm 10\%$ error interval. The blue shaded regions represent the mean of 95% confidence interval estimated using the Monte Carlo dropout method.

TABLE SIV. Evaluation and uncertainty of predictions for sample volumetric heat capacity (C_{sample}) and thermal conductivity (k_{sample}) by the machine learning model, incorporating the out-of-phase component of the third harmonic voltage as input.

Parameter	Evaluation		Uncertainty(%)	
	R^2	MAPE (%)	Mean	Standard deviation
C_{sample}	0.9937	2.020	5.577	1.045
k_{sample}	0.9984	1.345	7.292	0.986

Additionally, the machine learning model was applied to experimental data collected from a glass sample, incorporating both in-phase and out-of-phase components. The predicted results were a C_{sample} of 2.936 ± 1.029 [$\text{MJm}^{-3}\text{K}^{-1}$] and k_{sample} of 1.965 ± 1.807 [$\text{Wm}^{-1}\text{K}^{-1}$]. Figure S3 illustrates the theoretical curves derived from the predicted results alongside the experimental data points. Notably, the predicted curve shows significant deviation from the actual experimental results. Moreover, the uncertainty of predicted parameters by the dropout method shows significant values, suggesting the unreliability of the out-of-phase components in this context.

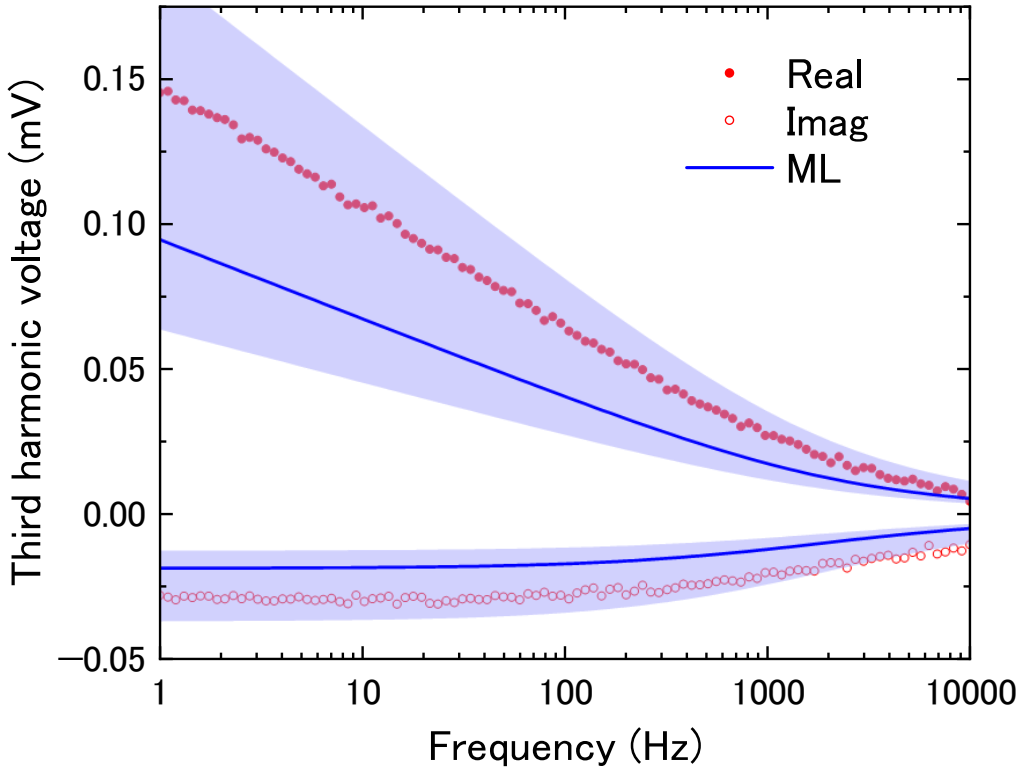

FIG. S3. Prediction results from the ML model for the three-omega measurement system, using input with the out-of-phase component of the third harmonic voltage. The shaded region around the blue solid line denotes prediction uncertainty, represented by the ±50% error interval in the fitted parameters.

7. Machine learning model for parylene substrate based three-omega sensor

To construct a database for the machine learning model associated with the parylene substrate-based three-omega sensor, each parameter was set according to Table SV. Notably, the thermal conductivity of parylene (k_{parylene}) was modeled as a function of its thickness of parylene (t_{parylene}) considering the size effects. This relationship was established by interpolating and extrapolating data from a previous study,[8] and the volumetric heat capacity was also based on these findings. The architecture for this machine learning model was outlined in Fig. S4, following the same process used in the two-layer model.

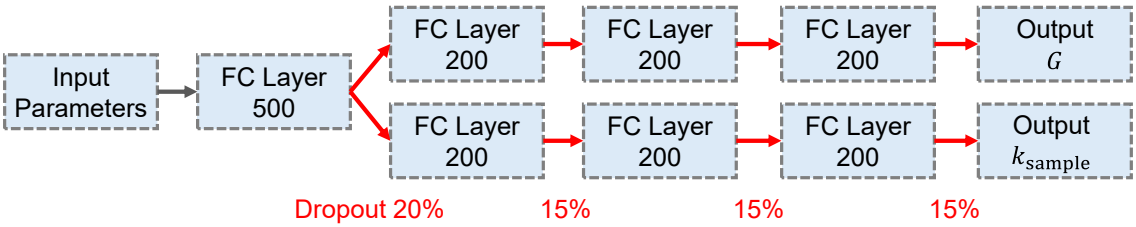

FIG. S4. Architecture of the neural network for the parylene substrate-based three-omega sensor measurement system.

TABLE SV. Physical parameters used in the database for the machine learning model concerning the parylene substrate-based three-omega sensor.

	Parameter	Range	Units
Constant	C_{air}	1.167	$\mathrm{kJm^{-3}K^{-1}}$
	k_{air}	0.0263	$\mathrm{Wm^{-1}K^{-1}}$
	C_{parylene}	918	$\mathrm{kJm^{-3}K^{-1}}$
	k_{parylene}	$f(t_{\mathrm{parylene}})$	$\mathrm{Wm^{-1}K^{-1}}$
Scaling	β^*	2200	ppm
	l^*	1	mm
	t^*_{heater}	100	nm
	ρ^*	2.35×10^{-8}	Ωm
	I^*_0	2	mA
Input	b	$2.0 - 10.0$	μm
	t_{parylene}	$0.1 - 1$	μm
	C_{sample}	$1.0 - 5.0$	$\mathrm{MJm^{-3}K^{-1}}$
Output	G	$0.1 - 100$	$\mathrm{MWm^{-2}K^{-1}}$
	k_{sample}	$0.1 - 100$	$\mathrm{Wm^{-1}K^{-1}}$

TABLE SVI. Evaluation and uncertainty of predictions for thermal boundary conductance (G) and sample thermal conductivity (k_{sample}) by the machine learning model for the parylene substrate-based three-omega sensor.

Parameter	Evaluation		Uncertainty (%)	
	R^2	MAPE (%)	Mean	Standard deviation
G	0.0431	28.85	16.65	11.16
k_{sample}	0.9936	1.653	6.160	1.150

The performance of the parylene substrate-based three-omega sensor model was evaluated using a test set, with results detailed in Table SVI. Figures S5(a) and S5(b) display each predicted value for thermal boundary conductance and thermal conductivity, respectively, relative to the true values. A comparative analysis of these predictions with those obtained from a fitting algorithm was also conducted, illustrated in Figs. S5(c) and S5(d) for thermal boundary conductance and thermal conductivity, respectively. The statistical outcomes of this comparison are presented in Table SVII.

In predicting thermal conductivity, as shown in Fig. S5(b), the machine learning model generally achieved precise predictions. When compared with the fitting algorithm, as illustrated in Fig. S5(d), differences do not appear to be significant in parylene substrate-based three-omega sensor model. This can be attributed to the low sensitivity of thermal boundary conductance, which makes the multiparameter fitting process highly dependent on thermal conductivity and relatively stable. However, there are notable discrepancies in the mean absolute percentage error (MAPE) and standard deviation, particularly because outliers cause significant errors, as observed in Table SVII.

For predictions of thermal boundary conductance, the accuracy declined significantly with increasing values, as depicted in Fig. S5(a). This trend can be attributed to the low sensitivity of thermal boundary conductance measurements, particularly as its influence on overall measurement diminishes with higher conductance values.

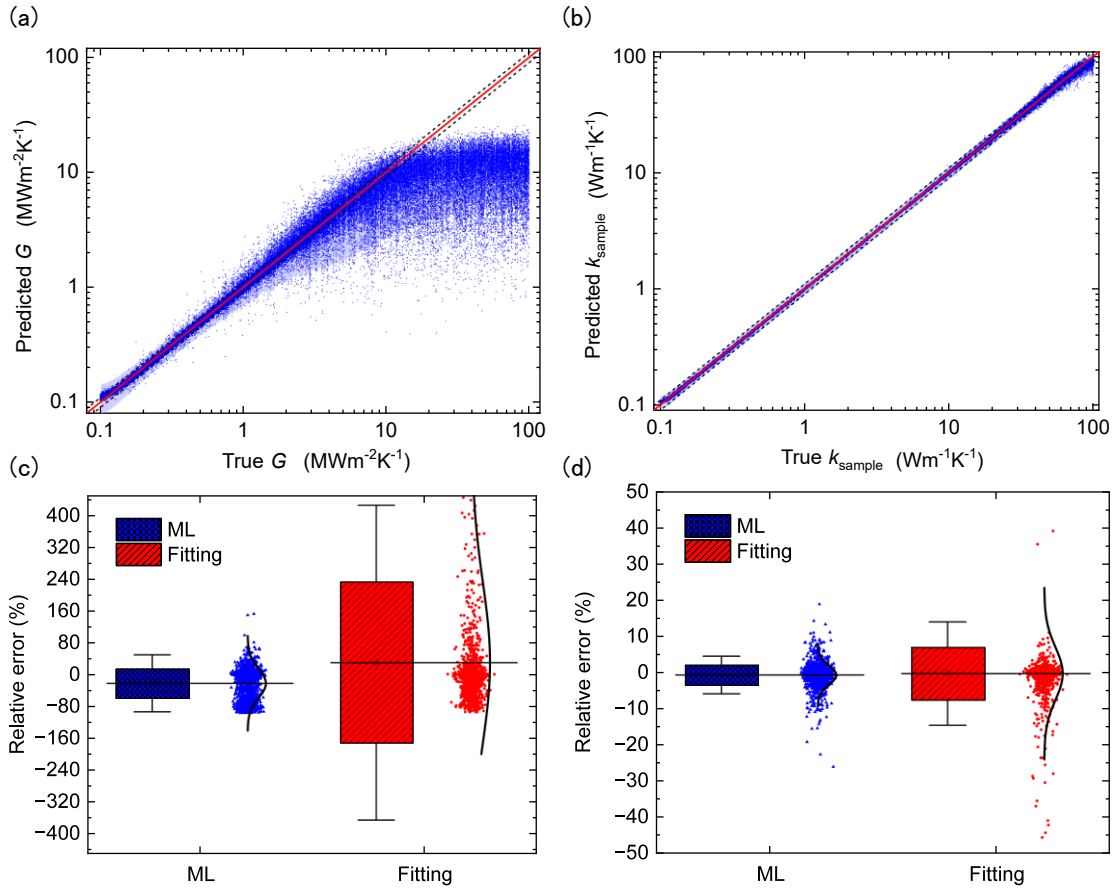

FIG. S5. Predictions from the machine learning model for (a) thermal boundary conductance (G) and (b) sample thermal conductivity (k_{sample}). Accurate predictions are indicated when points are close to the solid red line. The black dashed lines denote the $\pm 10\%$ error interval. The blue shaded regions correspond to the mean 95% confidence interval obtained via the Monte Carlo dropout method. Panels (c) and (d) compare the percentage error in predictions for thermal boundary conductance and thermal conductivity, respectively, between our machine learning model and conventional fitting methods.

TABLE SVII. Statistics of relative error in predictions for thermal boundary conductance (G), and sample thermal conductivity (k_{sample}) by ML and fitting algorithms for the parylene substrate-based three-omega sensor model, expressed in percentages.

	G		k_{sample}	
	ML	Fitting	ML	Fitting
Mean of percentage error	−22.33	33.06	−0.623	−0.307
MAPE	28.81	60.38	1.646	1.735
Standard deviation of relative error	36.45	234.0	2.643	7.268
Max absolute percentage error	151.3	4250	25.92	182.2

References

[1] S.J. Pan, and Q. Yang, "*A Survey on Transfer Learning*, " IEEE Trans. Knowl. Data Eng. **22**(10), 1345–1359 (2010).

[2] N. Srivastava, G. Hinton, A. Krizhevsky, I. Sutskever, and R. Salakhutdinov, "*Dropout: A Simple Way to Prevent Neural Networks from Overfitting*", J. Mach. Learn. Res. **15**(56), 1929–1958 (2015).

[3] Y. Gal, and Z. Ghahramani, "*Dropout as a Bayesian Approximation: Representing Model Uncertainty in Deep Learning*", in *Proc. 33rd Int. Conf. Mach. Learn.*, (2016) [DOI: arXiv:1506.02142].

[4] D.-A. Clevert, T. Unterthiner, and S. Hochreiter, "*Fast and Accurate Deep Network Learning by Exponential Linear Units (ELUs)*", (2016) [DOI: 10.48550/arXiv.1511.07289].

[5] K. He, X. Zhang, S. Ren, and J. Sun, "*Delving Deep into Rectifiers: Surpassing Human-Level Performance on ImageNet Classification*, " in *2015 IEEE International Conference on Computer Vision (ICCV)*, (IEEE, Santiago, Chile, 2015), pp. 1026–1034.

[6] D.P. Kingma, and J. Ba, "*Adam: A Method for Stochastic Optimization*", (2017) [DOI: 10.48550/arXiv.1412.6980].

[7] D.R. Lide, "*CRC Handbook of Chemistry and Physics*", CRC Press, (2000).

[8] A.A. Guermoudi, P.Y. Cresson, A. Ouldabbes, G. Boussatour, and T. Lasri, "*Thermal conductivity and interfacial effect of parylene C thin film using the 3-omega method*", J. Therm. Anal. Calorim. **145**(1), 1–12 (2021).